Phase Transition and Self-Assembly in Block Copolymers

Takeji Hashimoto

Department of Polymer Chemistry, Graduate School of Engineering, Kyoto University, Kyoto 606-8501, Japan, and Hashimoto Polymer Phasing Project, ERATO, JST, Japan

SUMMARY: We focussed on the following two topics on block copolymers; (i) the Brazovskii effects, effects of thermal fluctuations on phase transition of systems having a short characteristic length L, and (ii) nanofabrication and nanohybrids based on block copolymer nanostructures. We highlight the following two aspects: Block copolymers provide good model systems for studies of basic physical science and are useful for advanced functional materials and devices.

I. Introduction

Two decades ago, Leibler presented Landau-type mean-field theory for phase transition of block copolymers (bcps)[1]. This is a seminal theory that has greatly advanced basic science of bcps. The presented phase diagram elucidates the disordered phase where block chains are molecularly mixed and the ordered phase where various morphologies with long-range order are developed, depending on relative chain lengths of two blocks or fraction f of one of the block A in A-*b*-B block copolymer defined by $f = N_A/(N_A+N_B)$ where N_K is degree of polymerization (*DP*) of K-th block chain (K=A or B). The phase transition designated as microphase separation transition or order-disorder transition (ODT) is shown to be the first-order phase transition for asymmetric bcps with $f \neq 0.5$ but the second-order phase transition for bcps with $f = 0.5$ in the context of the mean-field (MF) theory. One of the unique features of this bcp system is that the characteristic length L of the microdomain structure in the ordered state is of the order of radius of gyration of bcp, R_g. Since the structure is very small, it will be strongly affected by thermal agitation, especially near the phase boundary.

Since presentation of the Leibler's theory, people investigated intensively the effects of thermal fluctuations on phase transition and self-organization process of bcps, partially because the effects are generally important on pattern formations in nature. Before presentation of the Leibler's MF theory, Bazovskii presented a general theory on the effects on phase transitions of systems having a small L[2]. However unfortunately this theory has not been extensively tested experimentally. We can approach this important basic problem by using bcps as an ideal model system, because in bcp $L \sim R_g \sim 10$ nm and dynamics are sufficiently slow due to a high viscosity of the system so that the ordering process is slow and

 CCC 1022-1360/00/$ 17.50+.50/0

hence can be relatively easily followed experimentally. As the basic physical science of bcps has been advanced[3-5], an increasing number of researchers has started to focus on applications of bcps for advanced functional and/or optoelectronic materials. Some aspect of the researches along this line will also be discussed briefly in the last part of this paper (sec. V).

II. A Review of Previous Works

We focus on symmetric or nearly symmetric bcps. What has been found so far is as follows: Thermal fluctuations change nature of phase transition of the bcp from the second-order to the first-order phase transition. This is called the fluctuation-induced first-order phase transition and has been theoretically elucidated first by Fredickson-Helfand[6] and experimentally by Bates and his coworkers[7]. These results clarified that the phase transition of bcps has the characteristics of Brazovskii universality class.

Now let us look at how the scattering from experimental systems with $f \cong 0.5$ (e.g., polystyrene-*block*-polyisoprene (SI) coded as OSI-3 with total number average molecular weight $M_n=1.5\times 10^4$ and heterogeneity index $M_w/M_n=1.02$, f for polystyrene (PS) block, f_{PS}, equal to 0.45) changes across ODT. Fig. 1 shows the inverse of the peak intensity I_m of small-angle X-ray scattering (SAXS) vs inverse absolute temperature T [8]. A discontinuous change is seen in I_m^{-1} vs T^{-1}between 100.2 ad 98.2°C, which manifests the fluctuation-induced ODT. The dotted line shows the MF behavior of I_m^{-1} vs T, predicted by the Leibler's theory[1]. Far above the ODT, the system is in the disordered state well approximated by this MF theory, but near ODT it is in the disordered state induced by thermal fluctuations. The MF theory predicts divergence of I_m toward infinity and hence drops of I_m^{-1} toward zero at spinodal temperature, defined here after as MF spinodal temperature $T_{S,MF}$. Below the $T_{S,MF}$, the disordered state should become thermodynamically unstable and therefore the system should order according to spinodal decomposition (SD), if the thermal fluctuations or agitations did not play an important role in the system. However the system remains

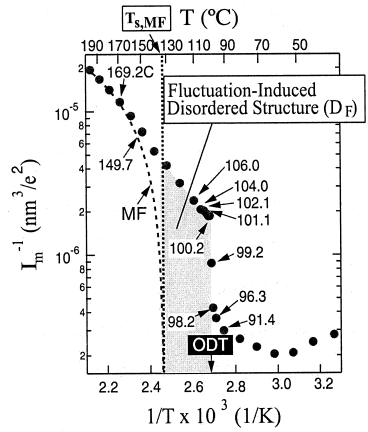

Figure 1: Inverse of the maximum SAXS intensity from the SI bcp (OSI 3) plotted as a function of inverse absolute temperature.

disordered even below $T_{S,MF}$ due to the thermal fluctuations preventing the system from ordering. Thus we have the fluctuation-induced disordered structure[9,10] in the temperature range between $T_{S,MF}$ and T_{ODT}, the ODT temperature. Upon lowering T below T_{ODT}, the system eventually undergoes a very sharp phase transition into the ordered lamellar phase. This is called fluctuation-induced first-order phase transition.

III. Fluctuation-induced Disordered Structure, D_F

Now what kind of structure do we have in between $T_{S,MF}$ and T_{ODT}? Lets us denote the structure as D_F, fluctuation-induced disordered structure. We have succeeded in vitrifying this D_F structure existing at T close to but above T_{ODT} by rapidly quenching it below Tg[9]. We confirmed the success in the vitrification process by finding that the SAXS profiles before and after quenching are identical. We further confirmed that the distribution of SAXS intensity with q itself was unchanged even after staining the frozen specimen with O_SO_4 , though the absolute scattered intensity was changed[9]. Thus the vitrified structure observed under TEM should really reflect the D_F structure existing *in-situ* at $T_{ODT} < T < T_{S,MF}$. Fig. 2 shows the typical D_F structure observed under TEM on the ultrathin sections of the vitrified specimens stained with O_SO_4[9]. The bright and dark phases represent the vitrified thermal composition fluctuations rich in PS and PI blocks, which are less stained and more stained, respectively. The inset shows a micrograph with a higher magnification. The dark and bright domains are uniformly distributed without a long-range order. This image is shown to reflect a frozen dynamical structure with no clear interface[9].

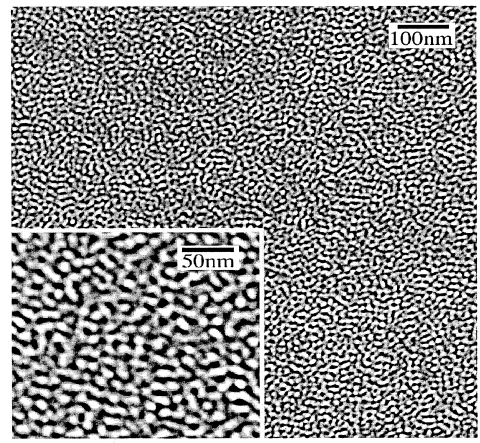

Figure 2: TEM observed for ultrathin sections of the films prepared by vitrifying the D_F structure existed at 100.2°C.

We conducted a theoretical analysis of this DF structure by using 2D computer simulation[10] based on time-dependent Ginzburg Landau model with Ohta-Kawasaki free energy functional[11]. The theory predicts that state of the system depends on two independent parameters: one is $\alpha \cong (\chi N)^{-2}$, related to the segregations power and the other $B \cong (\chi N)^{-1/2} N^{-1/2}$, strength of thermal noise where χ is the segmental interaction parameter and $N \equiv N_A + N_B$. The

MF assumes B=0 so that the system state depends only on α: the system changes from disordered state having a typical pattern (c) to an order state having the pattern (a) when α decreases below the MF critical value α_c= 0.25 or $(\chi N)_c$=10.495. Even in an ordered state with $\alpha < \alpha_c$, if we increase B, the system changes from the ordered phase with lamellar morphology (pattern a) to the disordered phase with the structure of pattern b[10]. This pattern well corresponds to the D_F structure found in our experiment.

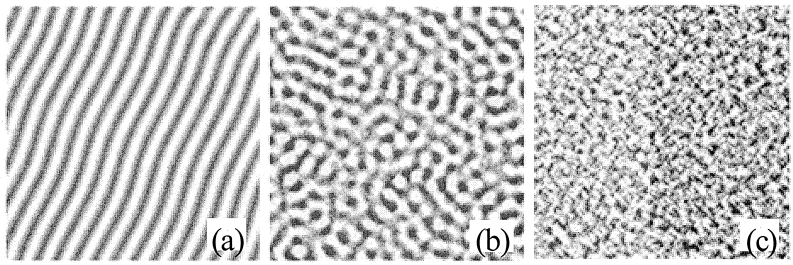

Figure 3: 2D computer simulation of the patterns based on TDGL equation with Ohta-Kawasaki free energy functional: (a) α=0.24, B=0, (b) α=0.24, B=0.01, (c) α=0.3, B=0.

IV. USAXS Studies of ODT

Now let us ask ourselves how sharp is this ODT? Generally the scattering profile from the ordered lamellae is very sharp, so that the conventional SAXS apparatus cannot always detect it accurately. In other words it is difficult for us to study rigorously the sharpness of the ODT with conventional SAXS apparatuses[12]. Therefore we used the Bonse-Hart type USAXS apparatus[13] for the analysis of the ordered lamella structure at a large length scale and/or with a high resolution. Our monochromator has a new design of a monolithic crystal with an asymmetric cut[14]. The apparatus covers a wide q-range of $0.002 < q < 0.5 nm^{-1}$ or length scale from 10 nm to 3 μm.

IV-1. Order-disorder coexistence as revealed by the USAXS method

Fig. 4 demonstrates typical USAXS profiles very near ODT from the SI bcp described in the caption, highlighting the profile only around the first-order scattering maximum[12]. At the highest temperature, we observe the very broad profile shown by filled triangles, typical to the scattering from the fully disordered phase. At the lowest temperature, we observe the very sharp profile shown by squares, typical to the scattering from the fully ordered state. At a temperature in between these two temperatures, we observe the profile shown by filled circles. It appears to be composed of a sharp component and a broad component, implying a

coexistence of the ordered and disorder phases. The small sharp spike at q centered around 0.35 nm^{-1} may be easily overlooked by experiments with conventional SAXS apparatuses. The scattering angles between the two successive data points here correspond only to 5 sec in arc, so that the scattering angles between the two data points at both edges of the spike correspond only to 30 sec arc. Here we make use of a high-resolution merit of USAXS. This profile was stable at least for 50hs, revealing that coexistence occurs at thermal equilibrium. We can fit the measured profile with a linear combination of a Gaussian function for the sharp component and a Lorentzian function for the broad component. We can determine the peak intensity I_m and half-width at half maximum of the peak (HWHM) σ_q for both the sharp component and broad component as a function of temperature. In the disordered state both σ_q and I_m^{-1} is large, while in the ordered state, they are small[12]. In the coexistence temperature range, σ_q and I_m^{-1} have two values, one for the disorder phase and the other for the order phase. The values change by about 2 orders of magnitude over the narrow temperature range of 2.2K so that the transition is found to be very sharp[12].

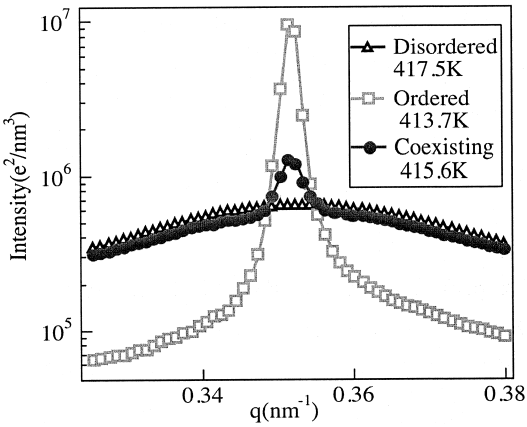

Figure 4: The USAXS profiles of the SI bcp coded as SS-7 (Mn=1.9×10^4, M_w/M_n=1.02, f_{PS}=0.46) near T_{ODT} at around q_m.

How can we theoretically interpret the biphase region at thermal equilibrium? A sound theoretical approach for disorder-to-order transition in bcps can be done with statistical mechanics based on an assembly of block copolymer chains (microscopic model). Instead of using this approach, we can coarse-grain the molecular assembly and describe the system based on order parameter $\psi(r)$, which is a spatial variation of composition of A or B block. According to this very powerful field theoretical approach (phenomenological model), the

amplitude of the order parameter ψ satisfies ψ=0 in the disordered state, while ψ spatially varies between +1, and −1 corresponding to A and B domains in the ordered phase, respectively. The order-disorder coexistence means that there is a region having ψ=0 and a region where ψ varies between +1 and −1 at thermal equilibrium.

We can give a qualitative interpretation[10] of the order-disorder coexistence based on Fredrickson-Helfand[6], Fredrickson-Binder[15] and Hohenberg-Swift (HS)[16] theories. In the field theoretical approach of HS, the free energy functional near ODT is expanded with respect to ψ, as given by eq.1 below,

$$F(\psi) = \int d\mathbf{r}\left\{\frac{\varepsilon}{2}\left[(\nabla^2 + q_0^{\,2})\psi(r)\right]^2 + \frac{\tau_0}{2}\psi(r)^2 + \frac{u_0}{4!}\psi(r)^4 + \frac{w_0}{6!}\psi(r)^6\right\} \qquad (1)$$

Where q_0 is wave number for a dominant mode of composition fluctuations, τ_0 is a parameter which depends on χN, while u_0 and w_0 are the parameters which depend only on Rg and f. In the context of the MF theory, the system in the ordered state has a negative value for τ_0, but positive value for u_0 and w_0, so that the free energy F of the system has double minima at ψ_0=+1 and −1 with respect to ψ_0, as shown in Fig. 5(a). Thus the single-phase state described by ψ_0=0 becomes thermodynamically unstable, and the system undergoes SD and phase-separates into two lamellar microphases having ψ_0=+1 or −1. When the thermal fluctuation effects are renormalized, the bare coefficients τ_0, u_0 and w_0 in eq. (1) change into τ, u, and w, respectively. Surprisingly enough, the coefficients τ becomes always positive, u becomes negative when the segregation power τ_0 is sufficiently large, and w is always positive[10]. Thus under a certain condition, the free energy curve F as a function of ψ can have triple minima and double maxima, as shown by the curve ② at ODT point[10]. This indicates a coexistence of the ordered phase having ψ_0=1 and −1 and the disordered phase having ψ_0= 0.

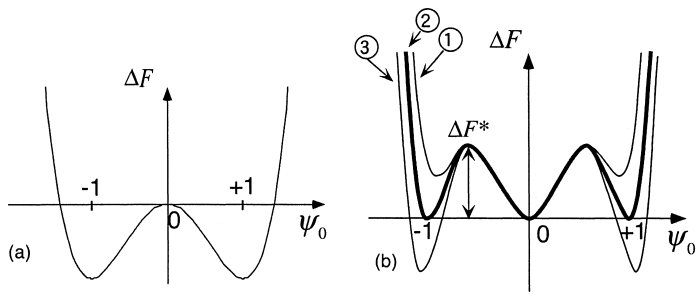

Figure 5: Free energy difference ΔF between the ordered and disordered phases in the MF approximation (a) and the non-MF (Hartree) approximation (b).

If thermal energy allows the system to jump over the free energy maximum ΔF^*shown in Fig. 5(b), then even under such a situation that the system is described by the curve ①, the ordered phase may coexist with the disordered phase at thermal equilibrium, although the population of the ordered phase is much less than that of the disordered phase, according to Boltzmann statistics. Hence the fluctuation-induced coexistence may occur over a certain finite temperature range[10]. We should note that in real world the order-disorder coexistence over a finite temperature range may be further promoted by molecular weight and composition distributions in bcps, investigations of which deserve future works. This renormalization group (RG) effect changes the system in thermodynamically unstable state in MF theory to a system in a metastable state. Note that the free energy maximum ΔF^* corresponds to a free energy barrier for nucleation and growth (NG) and that this barrier originates from the thermal fluctuations.

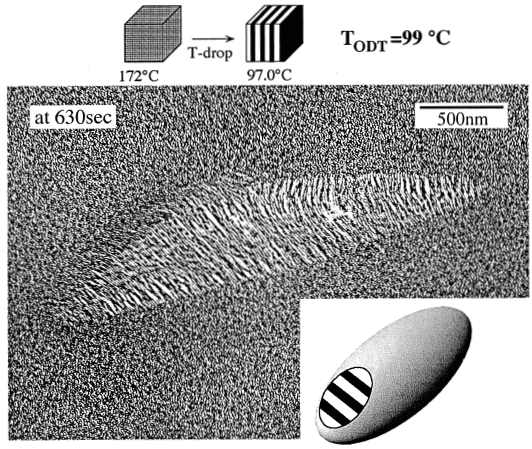

Figure 6: TEM showing the fluctuation-induced nucleation growth process. A highly anisotropic grain of ordered lamellae with their lamellar normals parallel to the long axis of the grain, as shown in the schematic model in the right bottom corner.

IV-2. Fluctuation-induced nucleation and growth

We succeeded in capturing TEM images showing nucleation of ordered grains of lamellae in the matrix of D_F structure as shown in Fig. 6 for the SI bcp (OSI-3) specimens[9, 17, 18] which were vitrified at 630s after being subjected to the ordering via NG at 97.0°C in the ordered state, slightly below T_{ODT}=100.2°C. The grains are highly anisotropic because of anisotropy of the interfacial tensions[17], and are developed after an induction period. We could reproduce this experimental finding by means of 2D computer simulation[17] based on TDGL theory with

the renormalized $F(\psi)$ given by HS[16]. After completion of ordering, TEM of the ordered lamellar phase is composed of many very anisotropic grains which are volume-filling. These anisotropic grains must originate from the fluctuation-induced NG of the ordered grains[9] having anisotropic shapes.

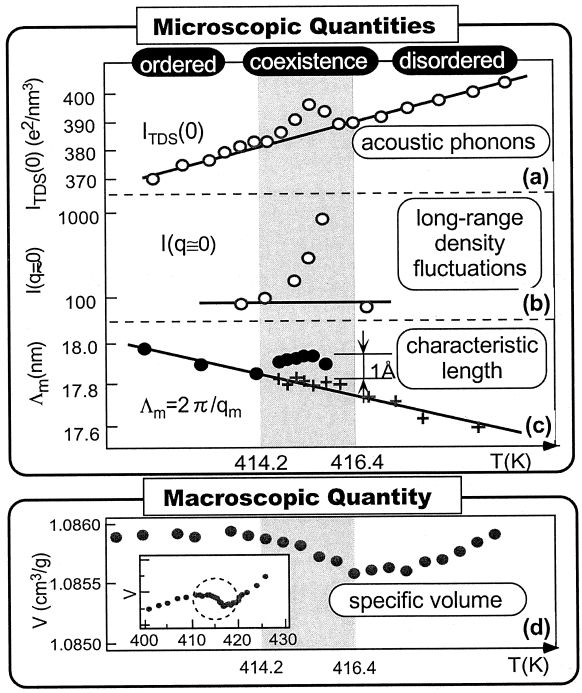

Figure 7: Anomalous behavior of $I_{TDS}(0)$, $I(q\cong 0)$, Λ_m, and specific volume in the order-disorder coexistence region observed for the SI bcp (SS-7).

IV-3. Anomalies in the order-disorder coexistence region

We found intriguing anomalies which exists only in the order-disorder coexistence region[12,19,20]. Let us next discuss these anomalies. Fig. 7 shows a summary of our results. We observe anomalies in the microscopic quantities, such as thermal diffuse scattering (TDS) intensity at $q= 0$, $I_{TDS}(0)$(part a), which is evaluated by extrapolation of SAXS intensity $I(q)$ from the intermediate q-range, the scattering intensity at $q\cong 0$, $I(q\cong 0)$(part b), measured with USAXS, and the characteristic length, Λ_m(part c), measured from q_m and a macroscopic quantity, for example, the specific volume(part d). Fig. 8 shows the method by which we estimated $I(q\cong 0)$, $I_{TDS}(0)$ and q_m. (a) The anomaly in TDS at q=0 reflects anomaly of acoustic phonons or isothermal compressibility[19].

$I_{TDS}(0)/\rho_{el} = \rho_{el} k_B T/\rho_m u_\ell^2$ (2), $\rho_m u_\ell^2 = (1+\frac{4}{3}\kappa_S G)/\kappa_T \cong 1/\kappa_T$ (3)

where ρ_{el} is electron density, ρ_m is mass density, u_ℓ is group velocity of phonons, κ_S is adiabatic compressibility, and κ_T is isothermal compressibility. (b) The anomaly in $I(q=0)$ reflects anomaly in the long-range density fluctuations[19]. (c) In the coexistence region, the characteristic length of the ordered phase is larger than that of the disordered phase by only 1 Å but this small expansion is reproducible and important[12, 20]. The inset in Fig. 7(d) shows the specific volume over a wide temperature range, while the main part of the figure highlights it only over a narrow region around T_{ODT}.

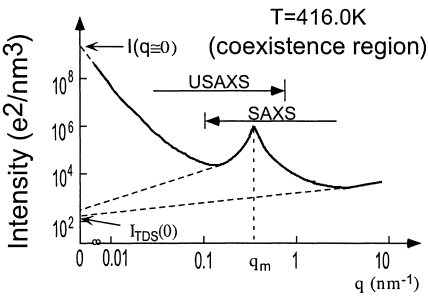

Figure 8: Combined USAXS and SAXS profiles from the SI bcp (SS-7) at 416 K in the order-disorder coexistence region. The figure defines $I(0)$, $I_{TDS}(0)$ and q_m.

We observe that all the anomalies occur only in the coexistence region[19]. Strikingly, the ordering of bcps is analogous to the ordering of water into ice: The ordering causes an increase of volume and an increase of the long-range density fluctuations as well, as seen in Fig. 7(b). This development of the large-length-scale density fluctuations is analogous to that in vitrification process of water or glass-forming liquid[21]. This bcp system can be brought into a complete ordering and the ordering causes suppression of the density fluctuations evolved in the coexistence region. However what happens, if this system is vitrified, before it completely orders. Then the density fluctuations will be frozen and remain in the system as in the case of glass-forming liquids.

Fig. 9 illustrates our model for the biphase structure in the order-disorder coexistence region. Our preliminary TEM results on the bcp specimens vitrified from the coexistence state by a rapid quenching of the specimens below T_g shows a coexistence of the network of the ordered lamellar phase and the disordered phase having D_F structure. We expect that there must be a small density difference between the two phases, which causes upturn

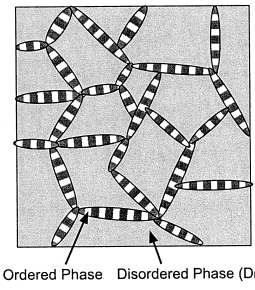

Figure 9: Schematic model for order-disorder coexistence.

in USAXS profiles as $q \rightarrow 0$ (see Fig. 8). The volume fraction of the ordered phase, X, is a function of T, and this density fluctuations disappear when X goes to either 1 or 0. This may be a reason why the large scale density fluctuations occur only in the coexistence region. In the vitrification process of water, this network corresponds to a temporal network of hydrogen-bonded water molecules[22], while in our bcp systems, this network corresponds to temporary network of ordered phase. Therefore the two very different systems show an intriguing similarity. In summary, the various anomalies found in our experiments provide new intriguing fundamental problems to be solved.

Let us now summarize the research accomplishments on the first topics, effects of thermal fluctuations on phase transition of bcps. Polymer science community contributed to basic physical science on the Brozovskii effects. It has shown both theoretically and experimentally that the thermal fluctuations change nature of phase transition from second-order to first-order. We have elucidated the fluctuation-induced disordered structure D_F, the fluctuation-induced order-disorder coexistence, unique anisotropic NG process, and anomalies in the order-disorder coexistence region. Especially, these anomalies are newly discovered and have not yet been theoretically verified and hence give new physical problems to be solved.

Before closing the first topics, we would like to point out "order-order phase transition" in bcps. Of course, we can tailor the nanopatterns by changing chemically the composition of two block chains. However, even a given bcp with a given composition can undergo order-order phase transition from one morphology to another, such as sphere, cylinder, bicontinuous, and lamella, just by changing temperature, pressure, and etc.[1, 6, 23-25] This order-order transition is also very interesting phase transition in bcp systems and enriches our methods to manipulate the self-assembling structures. There have been many excellent works reported along this line in recent years.

V. Fabrication of Nanopatterns in Block Copolymers

Let us now discuss some applications of nanopatterns of bcps for advanced devices.

The following studies may be pointed out as a few examples of the studies along this line:(a) tunable photonic crystals[27],(b) quantum dots and nanowires[28],(c) nanohybrids with inorganic materials[29], and (d) photovoltaics and photoluminescence.[30] Of course, there are many other interesting researches along this line. Objectives here are fabrication of nano-structures of bcps to create new materials with interesting nano-structures, and exploration of their methods and principles. Here we like to present some of our works on creation of

nanochannels in polymer matrix, oriented single-grain of nanopatterns, metal nanoparticles coordinated and stabilized by bcps, and nanohybrids between nanometal particles and polymer.

V-1. Nanochannels

Fig. 10(a) shows a computer graphic of the double gyroid network constructed on the basis of differential geometry[32]. In the graphic the two sets of gyroid networks are left empty and only the matrix phase exists. The cross-sectional view of (211) plane of the mathematical gyroid shows a set of periodically arranged bright waves having large and small amplitudes corresponding to the matrix phase as well as a gray zone corresponding to the empty network phase (Fig. 10(b)). These two patterns in Figs. 10(a) and 10(b) are the mathematical patterns calculated based on differential geometry[32], while the pattern in Fig. 10(c) is a pattern in the real world[31]. This pattern was obtained for an SI block copolymer films in which the PI phase was degraded into holes by ozonolysis. The degraded sample was freeze-fractured and its fractured surface was observed under SEM. This SEM pattern exactly reproduces the pattern predicted by differential geometry. In this way we could create 3D continuous, regular nanoholes or channels in the PS matrix. We could further plate the surface of this nanochannel with nickel through non-electrolytic plating process[31]. We think this is an interesting result in two senses: one from a view point of the nanofabrication and the other from a view point of fundamental science in that this result provides one of the most convincing evidence of the double gyroid network structure. This kind of patterns, which have been also found in lipid membranes, zeolites, etc.[32], can be relatively easily observed by using bcps as a model system.

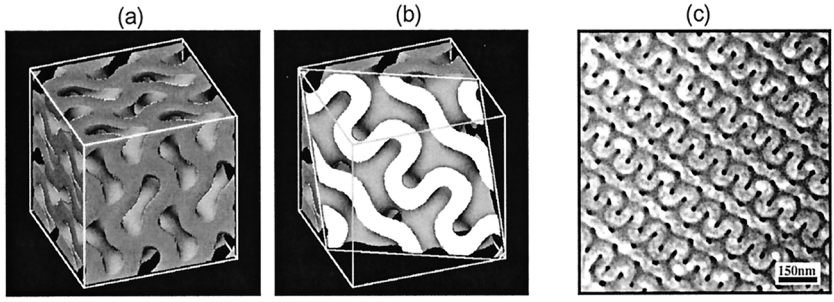

Figure 10: Computer graphic of double gyroid network (a) and its pattern appeared in the (211) plane (b). The SEM obtained from ozone-degraded PS-*b*-PI.

V-2. "Single crystals" of nanopatterns

Let us next discuss "superlamellae" created via "supertailoring". An artificial linking of polymer A and polymer B into A-B bcps enabled us to tailor unique nanostructures of given shapes and periodicity, as we have discussed already and as shown in the path way from Fig. 11(a) to 11(b). This is a chemical approach for tailoring the structure. If we further control physically the ordering process, we may be able to create a nanostructure with an oriented single-grain, as illustrated in Fig. 11(c). The combined physical and chemical approach, i.e., the path way from Fig. 11(a) to 11(c) may be called "super-tailoring" which may be useful for developing advanced optical and electronic devices.

As we have already discussed, a conventional ordering process of bcps occurs via NG, which eventually developed, for example, volume-filling lamellae composed of small grains having the anisotropic shape with a macroscopically random orientation (Fig. 11(b)). However if we combine ordering under moving temperature gradient and (glass) surface-induced ordering for the ordering process of lamella-forming bcps of SI, the ordering will progressively occur from the glass surface toward interior of the sample. Note that the glass surface is at the low T side and the interior is at the high T side, and the temperature gradient (∇T) moves from the glass surface to the interior. This process creates oriented single grain of lamellae, such as shown in Fig. 11(c), with their edges standing up with respect to film surfaces and with the vectors normal to the lamellar interfaces oriented parallel to ∇T [33].

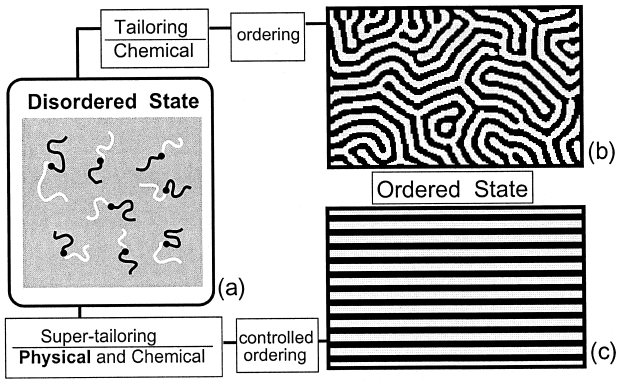

Figure 11: Tailoring of nanostructure via chemical approach (chemical linking of A and B polymers) vs "supertailoring" via physicochemical approach (chemical linking and controlled ordering).

We can easily distinguish between systems with many grains and those with a single grain by taking SAXS patterns with a two-dimensional (2D) detector. The 2D-SAXS pattern taken

with incident X-ray beam normal to the film specimen showed a series of sharp diffraction spots along the ∇T axis at the integer multiples of the first-order diffraction spot position, indicating that lamellae with their normals aligned parallel to the ∇T axis and with their edges standing up with respect to the film surfaces[34]. The diffracted intensity measured along the azimuthal angle showed a very sharp distribution, giving rise to the orientation factor of lamellar normals $f_{orient} \equiv [3 < \cos^2\alpha > -1]/2$, where α is the polar angle between the lamellar normal and the ∇T axis, is equal to 0.93[34),35)]. If we subtracted the background intensity due to the frozen thermal fluctuations of the lamella, f_{orient} becomes as high as 0.98. We have measured the area over which the single crystal grain exists by scanning a fine X-ray beam along the specimen with our synchrotron X-ray source at SPring 8, Nishiharima, Japan. We found that it extends up to 2mm along the direction normal to the glass surface and about 8 mm parallel to the grass surface[35)].

V-3. Hybrids of metal nanoparticles and block copolymers

Let us now discuss hybrids of metal nanoparticles and bcps. There will be, at least, two methods to prepare the hybrids as schematically shown in Fig. 12: one involves synthesis of stable metal nanoparticles first and then incorporation of them into microdomain space formed by bcps (method 1)[36,37] (Fig. 12(a)); the other involves formation of microdomain structure with metal ions and *in-situ* reduction of the ions in the microdomain space (method 2)[38] (Fig. 12(b)).

In method 1, we must first prepare metal nanoparticles coordinated and stabilized by polymers. For example, we can prepare palladium (Pd) metal particles of diameter 4 to 5 nm coordinated by poly(2 vinyl pyridine)(P2VP) homopolymer or poly(2 vinyl pyridine)-*block*-polyisoprene (P2VP-*b*-PI) by reducing Pd^{++} ions in dilute solution of the polymers. Most crucial problems to be solved here are: (a) how many chains are coordinating to the metals? ; (b) what kind of conformations the coordinating chains are taking? In our case we found that only a few bcp chains of P2VP-*b*-PI are coordinating Pd

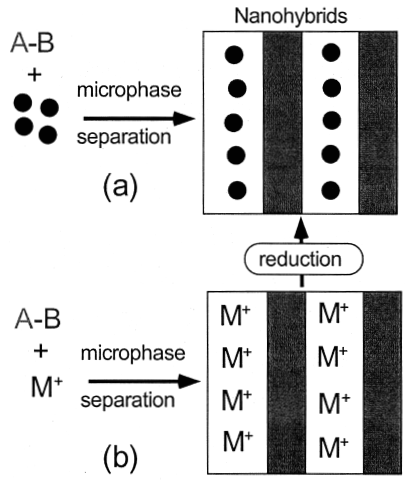

Figure 12: Incorporation of stabiliz nano-particles into microdomain.

nanoparticles from our AFM images[39] and that only a part of the chains is coordinating and a rest of the chains is free from the Pd particle[39]. These pieces of evidence imply that: (i) the Pd particle has a large fraction of free surfaces, and the polymer segments occupy only a minor fraction of the surface; nevertheless (ii) it is effectively stabilized by the coordinating polymers. In method 1, we incorporate thus prepared nanometals into the bcp nanospace. This method really involves a basic scientific problem concerning the self-assembly of the Pd nanoparticles coordinating bcps and the same bcps free from the particles, which provides the matrix space for the particles. We may be able to control a uniform distribution of the particles across the interface in one of the domains, a distribution of them along interface of the domain and a distribution of them along the middle of the microdomain space[37].

In method 2, which involves *in-situ* formation of nanometals in bcp microdomains, we first form microdomains in the solution of block copolymer containing Pd^{++} ions and alcohol as a reducing agent. Then metal ions are thermally reduced *in-situ* in the microdomain space to metal atoms at 85°C, for example. Here reduction of the metal ions and evaporation of solvent concurrently occur to result in formation of film containing microdomains and metal nanoparticles. The metal atoms reduced associate themselves into nanometal clusters via diffusion-coalescence process in viscoelastic medium of polymers. Fundamental scientific problems underlying this method will be as follows: (a) microdomain formation in the bcp systems containing the metal ions and the ion-polymer complex, (b) association of metal atoms and their growth in the viscous polymer matrix, and (c) location of metal clusters in the domains. An interesting approach for synthesizing hybrid silica nanostructures was developed by Wiesner and his coworkers[29], based on the same principle just described above.

Acknowledgements

The results presented here are mainly based on those obtained by Hashimoto Polymer Phasing Project, one of the ERATO (Exploratory Research for Advanced Technology) projects sponsored by Japan Science and Technology Corporation for which we gratefully acknowledge a financial support. We thank Drs. Tsuyoshi Koga, Tadanori Koga, Naoki Sakamoto, Yoshitsugu Hirokawa, Arimichi Okumura, Masafumi Harada, and Jeffery Bodycomb for their contributions to this work.

References

1. L. Leibler, *Macromolecules* **13**, 1602 (1980)
2. S.A. Brazovskii, *Soviet Phys. JETP* **41**, 85 (1975)
3. I. W. Hamley, *Block Copolymers*, Oxford U. P., Oxford, England (1999)
4. See for example, T. Hashimoto, *J. Polym. Sci. Polym. Phys.* **34**, 1819 (1996)
5. F. S. Bates, G. H. Fredrickson, *Physics Today* **52**, 32 (1999)
6. G. H. Fredrickson, E. Helfand, *J. Chem. Phys.* **87**, 697 (1987)
7. F. S. Bates, G. Fredrickson, *J. Chem. Phys.* **92**, 6255 (1990)

8. N. Sakamoto, T. Hashimoto, *Macromolecules* **28**, 6825 (1995)
9. N. Sakamoto, T. Hashimoto, *Macromolecules* **31**, 3815 (1998)
10. T. Hashimoto, T. Koga, T. Koga, N. Sakamoto, in: *The Physics of Complex Liquids*, F. Yonezawa, K. Tsuji, K. Kaji, M. Doi, T. Fujiwara (Eds.), World Scientific, Singapore 1988, p. 291 ff
11. T. Ohta, K. Kawasaki, *Macromolecules* **19**, 2621 (1986)
12. T. Koga, T. Koga, T. Hashimoto, *Phys. Rev. E.* **60**, R 1154 (1999)
13. U. Bonse, M. Hart, *Appl. Phys. Lett.* **7**, 238 (1965)
14. T. Koga, M. Hart, T. Hashimoto, *J. Appl. Cryst.* **29**, 318 (1996)
15. G. H. Fredrickson and K. Binder, *J. Chem. Phys.* **91**, 7265 (1989)
16. G. H. Hohenberg and J. B. Swift, *Phys. Rev. E.* **52**, 1828 (1995)
17. T. Hashimoto, N. Sakamoto, T. Koga, *Phys. Rev. E.* **54**, 5832 (1996)
18. N. Sakamoto, T. Hashimoto, *Macromolecules* **31**, 3292 (1998)
19. T. Koga, T. Koga, K. Kimishima, T. Hashimoto, *Phys. Rev. E.* **60**, R3501 (1999)
20. T. Koga, T. Koga, T. Hashimoto, *J. Chem. Phys.* **110**, 11076 (1999)
21. E. W. Fischer, *Physica A* **201**, 183 (1993)
22. S. Harrington, R. Zhang, P. H. Poole, F. Sciortino, and H. E. Stanley, *Phs. Rev. Lett.* **78**, 2409 (1997)
23. S. Sakurai, H. Kawada, T. Hashimoto, L. J. Fetters, *Proc. Jpn. Acad. (Ser. B)* **69**, 13 (1993); *Macromolecules* **26**, 5796 (1993)
24. D. A. Hajduk, S. M. Gruner, P. Rangarajan, R. A. Register, L. J. Fetters, C. Honeker, R. J. Albalak, E. L. Thomas, *Macromolecules* **27**, 490 (1994)
25. A. K. Khandpur, S. Förster, F. S. Bates, I. W. Hamley, A. J. Ryan, W. Bras, K. Almdal, K. Mortesen, *Macromolecules* **28**, 8796 (1995)
26. K. Kimishima, T. Koga, T. Hashimoto, *Macromolecules* **33**, 968 (2000)
27. A. Urbas, Y. Finkl, E. L. Thomas, *Macromolecules* **32**, 4748 (1999)
28. J. P. Spatz, A. Roescher, M. Moeller, *Advanced Materials* **8**, 337 (1996)
29. M. Templin, A. Frank, A. Du Chesne, H Leist, Y. Zhang, R. Ulrich, V. Schädler, U. Wiesner, *Science* **278**, 1795 (1997)
30. A. Hilberer, M. Moroni, R. E. Gill, H-J. Brouwer, V.V. Krasnikov, T.-A. Pham, G. G. Malliaras, S. Veenstra, M. L. Werts, P. F. van Hutten, G. Hadziioannou, *Macromol. Symp.* **125**, 99 (1997)
31. T. Hashimoto, K. Tsutsumi, Y. Funaki, *Langumuir* **13**, 6869 (1997)
32. See for example, S. Hyde, S. Andersson, K. Larsson, Z. Blum, T. Landh, S. Lidin, B. W. Ninham, *The Language of Shape*, Elsevier, Amsterdam, 1997
33. T. Hashimoto, J. Bodycomb, Y. Funaki, K. Kimishima, *Macromolecules* **32**, 952 (1999)
34. J. Bodycomb, Y. Funaki, K. Kimishima, T. Hashimoto, *Macromolecules* **32**, 2075 (1999)
35. J. Bodycomb and T. Hashimoto, in preparation
36. K. Tsutsumi, Y. Fnaki, Y. Hirokawa, and T. Hashimoto, *Langmuir* **15**, 5200 (1999)
37. A. Okumura, K. Tsutsumi, T. Hashimoto, *Polym. J.* **32**, 520 (2000)
38. T. Hashimoto, M. Harada, N. Sakamoto, *Macromolecules* **32**, 6867 (1999)
39. D. Tanabe, A. Okumura, T. Hashimoto, in preparation